Published in final edited form as:

Inorg Chem. 2015 January 5; 54(1): 273–279. doi:10.1021/ic502414r.

Heterobimetallic Complexes of Rhodium Dibenzotetramethylaza[14]annulene [(tmtaa)Rh-M]: Formation, Structures, and Bond Dissociation Energetics

Gregory H. Imler, **Garvin M. Peters**, **Michael J. Zdilla***, and **Bradford B. Wayland***

Department of Chemistry, Temple University, 1901 North 13th Street, Philadelphia, Pennsylvania 19122, United States

Abstract

A rhodium(II) Dibenzotetramethylaza[14]annulene dimer ([(tmtaa)Rh]$_2$) undergoes metathesis reactions with [CpCr-(CO)$_3$]$_2$, [CpMo(CO)$_3$]$_2$, [CpFe(CO)$_2$]$_2$, [Co(CO)$_4$]$_2$, and [Mn-(CO)$_5$]$_2$ to form (tmtaa)Rh-M complexes (M = CrCp(CO)$_3$, MoCp(CO)$_3$, FeCp(CO)$_2$, Co(CO)$_4$, or Mn(CO)$_5$). Molecular structures were determined for (tmtaa)Rh-FeCp(CO)$_2$, (tmtaa)Rh-Co(μ-CO)(CO)$_3$, and (tmtaa)Rh-Mn(CO)$_5$ by X-ray diffraction. Equilibrium constants measured for the metathesis reactions permit the estimation of several (tmtaa)Rh-M bond dissociation enthalpies (Rh—Cr = 19 kcal mol^{-1}, Rh—Mo = 25 kcal mol^{-1}, and Rh—Fe = 27). Reactivities of the bimetallic complexes with synthesis gas to form (tmtaa)Rh-C(O)H and M-H are surveyed.

Graphical abstract

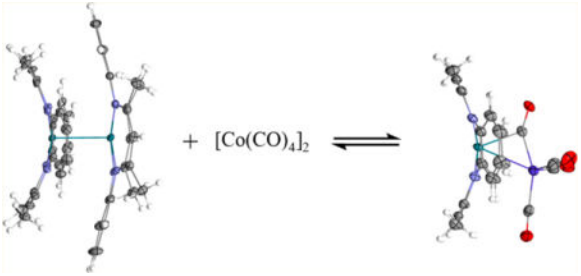

INTRODUCTION

The easily prepared, low cost N_4^{2-} macrocyclic ligand Dibenzotetramethylaza[14]annulene dianion (tmtaa) has been suggested as a substitute for porphyrins.[1–3] A rhodium(II) tmtaa dimer ([(tmtaa)Rh]$_2$, **1**) has recently been reported to react with synthesis gas (H_2/CO) in toluene and pyridine to form large equilibrium concentrations of a metallo-formyl complex

***Corresponding Authors:** mzdilla@temple.edu; bwayland@temple.edu.

Supporting Information

Solution spectra, equilibrium measurements, full crystallographic tables, and crystallographic information files (cif). This material is available free of charge via the Internet at http://pubs.acs.org.

Notes

The authors declare no competing financial interests.

((tmtaa)Rh-C(O)H) (Figure 1).[3] Rhodium(II) porphyrins and related chelates and macrocycles provide precedents for reactions of H_2/CO that produce η^1-carbon-bonded formyl complexes.[4–17] Several approaches attempting to advance the utilization of this type of metal-formyl fragment in the production of organic oxygenates invoke reactions that occur at the formyl group, such as hydrogenation using a second catalyst.[18,19] Bimetal catalyst systems for alkene hydroformylation that involve intermolecular processes illustrate the efficacy of this type of strategy.[20–22] Heterobimetallic complexes can be anticipated to occur in bimetal catalyst systems as nonproductive traps for active metal catalyst species. Reactivity studies of bimetallic compounds are important to determine whether or not these intermetallic intermediates are capable of returning the active catalyst units back into the productive cycle.

This Article reports on the formation, structural features, and dissociation energetics for a series of bimetallic complexes ((tmtaa)Rh-M) produced by metathesis reactions of [(tmtaa)-Rh]$_2$ (**1**) with [CpCr(CO)$_3$]$_2$ (**2**), [CpMo(CO)$_3$]$_2$ (**3**), [CpFe(CO)$_2$]$_2$ (**4**), [Co(CO)$_4$]$_2$ (**5**), and [Mn(CO)$_5$]$_2$ (**6**). Minimum energy structure optimized density functional theory (DFT) computations reproduce the primary structural features of the bimetal complexes, including an unexpected semi-bridging carbonyl in the molecular structure of (tmtaa)Rh-Co(μ-CO)(CO)$_3$.

RESULTS AND DISCUSSION

The closed shell dimers [CpCr(CO)$_3$]$_2$, [CpMo(CO)$_3$]$_2$, and [Mn(CO)$_5$]$_2$, which have only terminal CO ligands, are unambiguously described as having M–M bonds, but the presence of bridging CO units complicates the description of the bonding in [CpFe(CO)$_2$]$_2$ and [Co(CO)$_4$]$_2$[23,24] Each of these dimers can homolyze to a metal-centered radical,[25] and for the purpose of unifying and simplifying the presentation in this Article, all of the dimers (**2**–**6**) will be described as if the M–M bond were present.

Toluene solutions of the Rh^{II}–Rh^{II} bonded dimer (**1**) undergo metathesis reactions with **2**, **3**, **4**, **5**, and **6** to produce equilibrium distributions with heterobimetallic complexes of the general form (tmtaa)Rh-M, where M = CpCr(CO)$_3$ (**7**), CpMo(CO)$_3$ (**8**), CpFe(CO)$_2$ (**9**), Co(CO)$_4$ (**10**), and Mn(CO)$_5$ (**11**), respectively (eq 1).

$$[(\mathrm{tmtaa})\,\mathrm{Rh}]_2 + \mathrm{M}-\mathrm{M} \rightleftharpoons 2\,(\mathrm{tmtaa})\,\mathrm{Rh}\text{-}\,\mathrm{M} \quad (1)$$

Reactions of dimers **2**–**6** usually involve thermal or photo homolysis to form monomeric d^5, d^7, and d^9 metal-centered radicals. Thermal homolysis of compounds **1**–**6** into monomers occurs with reported dissociation enthalpies ranging from 15.5 to 33 kcal mol^{-1}.[2,26–28] Thermal reactions of the more strongly bonded dimer species that pass through metallo-radicals are slow because the dissociation enthalpies directly contribute to the activation parameters. Kinetics of the dimer reactions are often greatly increased by light-induced dimer homolysis. Both the π to σ^* and the σ to σ^* electronic transitions associated with M–M single-bonded complexes place an electron in the antibonding M–M σ molecular orbital and give photoinduced dimer homolysis.[29]

The lowest energy pathway for metathesis reactions of the form in reaction **1** is most likely a radical chain reaction that proceeds through an associative radical interchange (eqs 2, 3).[30,31] The Rh(II) center in $[(tmtaa)Rh]_2$ is a 5-coordinate, 16-electron site that can bind to M● and facilitate radical interchange (eqs 2, 3).

$$M - M \rightleftharpoons 2M\bullet \quad (2)$$

$$M\bullet + [(tmtaa)Rh]_2 \rightleftharpoons M\text{-}\ Rh(tmtaa) + (tmtaa)Rh\bullet \quad (3)$$

Formation and Reactions of (tmtaa)Rh-CrCp(CO)$_3$

Reaction of $[(tmtaa)Rh]_2$ (**1**) in toluene with a three-fold excess of $[CpCr(CO)_3]_2$ (**2**) produces a ^{1}H NMR-measurable equilibrium with the metathesis product $CpCr(CO)_3$ (7) (K_4 = 0.19 (0.05), $\Delta G_4°$ = 0.98 kcal mol^{-1}) (eq 4) in a period of hours at 298 K in the absence of light.

$$[(tmtaa)Rh]_2 + [CpCr(CO)_3]_2 \rightleftharpoons 2\,(tmtaa)Rh\text{-}\ CrCp(CO)_3 \quad (4)$$

Reaction 4 is relatively fast for this type of process when light is absent. The dissociation free enthalpy for **2** is small (15.5 kcal mol^{-1}),[27] which makes **2** a facile source of $Cp(CO)_3Cr$●, but reaction 4 is observed to be further accelerated by visible and UV irradiation.

The temperature dependence of $\Delta\nu_{1/2}$ (Hz) for the η^5-cyclopentadienyl ligand hydrogens in (tmtaa)Rh-CrCp(CO)$_3$ is shown in Figure 2. The observed increase in the η^5-Cp ^{1}H NMR full line width at half height for (tmtaa)Rh-CrCp(CO)$_3$ as the temperature is elevated is ascribed to lifetime broadening that results from dissociation of the diamagnetic (tmtaa)Rh-CrCp(CO)$_3$ complex into paramagnetic (S = 1/2) metal-centered radicals (tmtaa)Rh● and ●CrCp(CO)$_3$.

The observed ^{1}H NMR line width ($\Delta\nu_{1/2(obs)}$) is given as the sum of the natural line width and the line width resulting from dissociation into paramagnetic components ($\Delta\nu_{1/2(obs)} = \Delta\nu_{1/2(nat)} + \Delta\nu_{1/2(ex)}$). Equation 5 gives the general relationship of the contribution of this exchange to the NMR line width ($\Delta\nu_{1/2(ex)}$) with the electron–proton coupling constant (A_H) and the diamagnetic (τ_d) and paramagnetic lifetimes (τ_p). Equation 5 simplifies to eq 6 ($T_2^{-1} = k_{ex}$) for the case in which each exchange event results in nuclear spin relaxation. This limiting case occurs when the electron–nuclear coupling constant (A) is large enough such that $(A\tau_P/2)^2 \gg 1$.

$$\pi\Delta\nu_{1/2(ex)} = T_2^{-1} = \tau_d^{-1}[(A_H\tau_P/2)^2]\,[1+(A_H\tau_P/2)^2]^{-1} \quad (5)$$

$$\pi\Delta\nu_{1/2(\mathrm{ex})}=T_2^{-1}=\tau_\mathrm{d}^{-1}=k_\mathrm{ex} \quad (6)$$

The mean lifetime for the diamagnetic species (τ_d) that results from the observed T_2^{-1} yields the apparent rate constant ($\tau_\mathrm{d}^{-1} = k_\mathrm{ex}$) for bond homolysis events that produce paramagnetic species with efficient nuclear relaxation ($(A\tau_\mathrm{p}/2)^2 \gg 1$). Activation parameters for homolytic dissociation of (tmtaa)Rh-CrCp(CO)$_3$ were obtained by application of transition state theory ($K^{\ddagger} = k_\mathrm{ex}(h/kT)$; $-RT\ln K^{\ddagger}_\mathrm{ex} = \Delta G^{\ddagger} = \Delta H^{\ddagger} - T\Delta S^{\ddagger}$).[6,32–36] Using a $\Delta\nu_{1/2(\mathrm{nat})}$ of 1.0 Hz for the Cp hydrogens of 7 yields the apparent activation parameters of $\Delta H^{\ddagger}$ = 21 (1) kcal mol^{-1} and $\Delta S^{\ddagger}_{\mathrm{ex},4}$ = 19.6 (1.2) cal K^{-1} mol^{-1} for homolytic dissociation of (tmtaa)Rh-CrCp(CO)$_3$ (Figure 3). Activation enthalpies for homolytic bond dissociation ($\Delta H^{\ddagger}_\mathrm{app}$) in a low viscosity medium like toluene are about 2 kcal mol^{-1} larger than the bond dissociation enthalpies (BDE; $\Delta H°$),[34,35,37,38] which places the Rh-Cr BDE in (tmtaa)Rh-CrCp(CO)$_3$ at ~19 kcal mol^{-1}.

An estimate for the Rh-Cr BDE in (tmtaa)Rh-CrCp(CO)$_3$ is alternately obtained from the equilibrium studies in toluene for reaction 4. Using $\Delta G_4°$ (298 *K*) of 0.98 kcal mol^{-1}, Rh(II)-Rh(II) BDE for [(tmtaa)Rh]$_2$ of 22 kcal mol^{-1}, and [CpCr(CO)$_3$]$_2$ Cr–Cr BDE of 15.5 kcal mol^{-1},[27] and assuming that $\Delta S_4°$ is approximately zero, results in an estimate of 18 kcal mol^{-1} for the Rh-Cr BDE compared to 19 kcal mol^{-1} estimated by bond homolysis kinetics (Figure 3).

Exhaustive efforts to obtain single crystals of (tmtaa)Rh-CrCp(CO)$_3$ for X-ray diffraction were unsuccessful. The small equilibrium constant for reaction 4 precluded obtaining (tmtaa)Rh-CrCp(CO)$_3$ in the absence of [(tmtaa)Rh]$_2$ and [CpCr(CO)$_3$]$_2$, which reduced the probability of obtaining a crystal of **7**. Fourier transform infrared spectroscopy (FTIR) for a KBr pellet of the reaction mixture containing (tmtaa)Rh-CrCp(CO)$_3$ shows a new CO stretching band at 1766 cm^{-1} that is indicative of an intermetal-bridging CO unit. DFT calculations[39] were carried out using the B3LYP functional and a mixed basis set (6-31G* for C, H, N, O, and Cr; 3-21G for Rh) for (tmtaa)Rh-CrCp(CO)$_3$. DFT computations for **7** starting from an all-terminal CO structure reached a computed minimum energy structure that contains a bridging CO unit consistent with the CO stretching frequency of 1766 cm^{-1} (Figure 4). Calculated Mulliken atomic charges from DFT show a smaller positive charge on the carbon of the semibridging CO (C = 0.197, O = −0.317) compared to that of the terminal CO units (C_avg = 0.257, O_avg = −0.320).

Toluene solutions of **7** with [(tmtaa)Rh]$_2$ and [CpCr-(CO)$_3$]$_2$ in a vacuum-adapted NMR tube were charged with 1.0 atm of a 1:1 molar mixture of H_2 and CO, and changes in the solution composition were followed by ^{1}H NMR. At these conditions, **7** is fully consumed to form (tmtaa)Rh-C(O)H and [CpCr(CO)$_3$]$_2$ (eq 7). There are mutiple pathways to accomplish this transformation, but the distribution of species is defined by equilibria described by eqs 7–9.

$$(\mathrm{tmtaa})\,\mathrm{Rh\text{-}\ CrCp(CO)_3} + \mathrm{H_2} + 1/2\mathrm{CO} \rightleftharpoons (\mathrm{tmtaa})\mathrm{Rh\text{-}\ C(O)H} + \mathrm{H\text{-}\ CrCp(CO)_3} \quad (7)$$

$$(\mathrm{tmtaaRh{-}H} + \mathrm{CO} \rightleftharpoons (\mathrm{tmtaaRh{-}C(OH} \quad (8)$$

$$[\,\mathrm{CpCr(CO)_3}]_2 + \mathrm{H_2} \rightleftharpoons 2\mathrm{Cp(CO)_3Cr{-}H} \quad (9)$$

The equilibrium constant for the reaction of (tmtaa)Rh-H with CO (eq 8) to produce a rhodium formyl complex (tmtaa)Rh-C(O)H in toluene ($K_{8(298\ K)}$ = (10.8 (0.3)) × 10^3, $\Delta G_8°$ (298 *K*) = −5.5 kcal mol^{-1}) is sufficiently large such that at a pressure of 0.5 atm of CO the conversion of (tmtaa)Rh-H to the formyl complex (tmtaa)Rh-C(O)H is effectively complete, and the (tmtaa)Rh-H concentration is too small for observation by ^{1}H NMR.[3] Favorable thermodynamics for reaction 9 also give high conversion of $[CpCr(CO)_3]_2$ to $Cp(CO)_3Cr$-H at a pressure of 0.5 atm of H_2 at 298 K.[40]

Formation and Reactions of (tmtaa)Rh-MoCp(CO)$_3$

Reaction of $[(tmtaa)Rh]_2$ (**1**) with $[CpMo(CO)_3]_2$ (**3**) in the absence of light slowly produces a ^{1}H NMR observable equilibrium with (tmtaa)Rh-$MoCp(CO)_3$ (**8**) over a period of days (eq 10). Reaction 10 is greatly accelerated by light and reaches completion in a period of minutes when carried out in a Rayonet RMR-400 photochemical reactor with a 300 nm light source.

$$[(\mathrm{tmtaa})\,\mathrm{Rh}]_2 + [\mathrm{CpMo(CO)_3}]_2 \rightleftharpoons 2(\mathrm{tmtaa})\mathrm{Rh\text{-}\ MoCp(CO)_3} \quad (10)$$

A BDE for Rh-Mo of 25 kcal mol^{-1} is estimated for **8** from the equilibrium constant for reaction 10 at 298 K in toluene ($K_{10(298\ K)}$ = 7.8 × 10^{-2}, $\Delta G_{10}°$ (298 K) = 1.5 kcal mol^{-1}) along with the Rh–Rh and Mo–Mo BDEs for $[(tmtaa)Rh]_2$ (22 kcal mol^{-1})[2] and $[CpMo(CO)_3]_2$ (30 ± 3 kcal mol^{-1}),[26] respectively. The Rh-Mo BDE in (tmtaa)Rh-$MoCp(CO)_3$ is estimated at 25 ± 3 kcal mol^{-1} assuming that $\Delta S_{10}°$ is close to zero. The Rh-Mo BDE in **8** is about 7 kcal mol^{-1} larger than the Rh-Cr BDE in **7**, which is in the range expected for second transition series metal complexes compared to analogous first transition series metal species. Minimum energy structural optimization by DFT (B3LYP, 3-21G)[39] anticipates a semi-bridging carbonyl in complex **8** (Figure 5), and calculated Mulliken atomic charges for this unit show a smaller positive charge on the semibridging CO (C = 0.162, O = −0.312) compared to that of the terminal CO units (C_{avg} = 0.201, O_{avg} = −0.305).

Solutions of **3** in equilibrium with **1** and **8** in toluene were charged with 706 Torr of a 50:50 mixture of CO/H_2, and the subsequent slow reactions were followed by ^{1}H NMR for a

period of weeks. When the sample reached equilibrium through reactions 8, 11, and 12, compounds **3**, (tmtaa)Rh-C(O)H, and $Cp(CO)_3Mo$-H were observed in the ^1H NMR spectrum.

$$(\mathrm{tmtaa})\,\mathrm{Rh\text{-}\ MoCp(CO)_3} + \mathrm{H_2} + 1/2\mathrm{CO} \rightleftharpoons (\mathrm{tmtaa})\mathrm{RhC(O)H} + \mathrm{Cp(CO)_3Mo\text{-}\ H} \quad (11)$$

$$[\,\mathrm{CpMo(CO)_3}]_2 + \mathrm{H_2} \rightleftharpoons 2\mathrm{Cp(CO)_3Mo{-}H} \quad (12)$$

The equilibrium constant for the reaction of $[CpMo(CO)_3]_2$ with H_2 to form $Cp(CO)_2Mo$-H (eq 12) was evaluated by integration of the ^1H NMR ($K_{12(298\ K)} \cong 1.7$; $\Delta G_{12}°$ (298 K) ≅ −0.3 kcal mol^{-1}). An estimate of 67 (3) kcal mol^{-1} for the Mo-H BDE in $Cp(CO)_2Mo$-H is obtained by using a Mo–Mo BDE of 30 (3) kcal mol^{-1} for $[CpMo(CO)_3]_2$ along with an H–H BDE of 104 kcal mol^{-1} and using $\Delta H_{12}° \cong \Delta G_{12}°$ (298 K).[26] This estimate of 67 (3) kcal mol^{-1} for the Mo-H BDE in $Cp(CO)_2Mo$-H compares favorably with prior published estimates in the range of 66–69 kcal mol^{-1}.[41,42] The Mo-H BDE is ~7 kcal mol^{-1} larger than the Cr-H BDE in $Cp(CO)_2M$-H, which is in the range expected for second versus first transition series metal hydrides.

The rhodium formyl complex ((tmtaa)Rh-C(O)H) is the only observed product that contains the (tmtaa)Rh unit because $K_{8(298\ K)}$ is very large. Removing H_2/CO gases from solution by three freeze–pump–thaw cycles results in the formyl complex completely reverting to a mixture of **1** and **8** during a period of one week, but $Cp(CO)_3Mo$-H did not decrease at an observable rate over this time. Reaction of $[MoCp(CO)_3]_2$ with 700 Torr of a 50:50 mole fraction ratio of CO/H_2 in the absence of **1** did not produce ^1H NMR-observable concentrations of $Cp(CO)_3Mo$-H over a period of one week. Thermal reaction of $[MoCp(CO)_3]_2$ with H_2/CO must be catalyzed by the presence of a (tmtaa)Rh species such as (tmtaa)Rh-H.

Formation and Reactions of (tmtaa)Rh-FeCp(CO)$_2$

Toluene solutions of $[(tmtaa)Rh]_2$ (**1**) in the absence of light react very slowly with excess $[\eta^5\text{-}CpFe(CO)_2]_2$ (**4**) over 18 days to produce an equilibrium distribution with the heterobimetallic complex (tmtaa)Rh-$FeCp(CO)_2$ (**9**) (eq 13). Reaction 13 is accelerated in ambient laboratory light, and the reaction is completed after irradiation for 10 min in a Rayonet RMR-400 photochemical reactor with a 300 nm source.

$$[(\mathrm{tmtaa})\,\mathrm{Rh}]_2 + [\mathrm{CpFe(CO)_2}]_2 \rightleftharpoons (\mathrm{tmtaa})\,\mathrm{Rh{-}FeCp(CO)_2} \quad (13)$$

Crystals of heterobimetallic complex in solutions of **9** were grown from slow diffusion of pentane in toluene, and the molecular structure was determined by single crystal X-ray diffraction. An ORTEP diagram for **9** at the 50% probability level is shown in Figure 6 along

with an energy-minimized structure from DFT computations (B3LYP, 3-21G/6-31G*). The presence of a d^7–d^7 Rh^{II}-Fe^{I} bond (263 nm), an η^5-Cp, and all terminal CO ligands are the primary structural features observed in the molecular structure. The energy-minimized structure from DFT (B3LYP, 3-21G/6-31G*)[39] computations also shows all of the most important structural features for **9** (Figure 6).

Dihedral angles looking down the N-$C_{benzene}$ single bond of tmtaa in **9** show an inequivalency present in the ligand with larger dihedral angles (31.8°) in the half of tmtaa opposite the Cp ligand on iron and smaller dihedral angles (23.4°) on the alternate half. These dihedral angles define the tilting of the nonplanar saddle shape of the tmtaa macrocycle, and the inequivalency here shows that there is more pronounced tilting of the diiminato fragment on one-half of tmtaa to accommodate the steric demands of the η^5-Cp ligand on iron.

The equilibrium constant for reaction 13 was directly evaluated by integration of the ^{1}H NMR for each species in reaction 13 ($K_{13(298\ K)}$ = 0.19; $\Delta G_{13}°$ (298 K) = 0.98 kcal mol^{-1}). An estimate of 27 (5) kcal mol^{-1} for the Rh-Fe BDE in (tmtaa)Rh-FeCp(CO)$_2$ is obtained by using the Rh–Rh BDE of 22 kcal mol^{-1} for [(tmtaa)Rh]$_2$ and the electrochemical estimate for the Fe–Fe BDE for [CpFe(CO)$_2$]$_2$ (33 ± 5 kcal mol^{-1})[26] and assuming that $\Delta H_{13}° \cong \Delta G_{13}°$ = 0.98 kcal mol^{-1}.

Formation of (tmtaa)Rh-Co(μ-CO)(CO)$_3$

Reaction of [(tmtaa)Rh]$_2$ (**1**) with an excess of [Co(CO)$_4$]$_2$ (**5**) in toluene occurs immediately and completely to form (tmtaa)Rh-Co(μ-CO)(CO)$_3$ (**10**). Excess [Co(CO)$_4$]$_2$ was removed by evacuation of the toluene solution followed by vacuum sublimation; however, subsequent IR (KBr pellet) showed traces of dicobalt octacarbonyl remaining. The reverse reaction of **10** to form **1** and **5** was not observed after removing most of the excess [Co(CO)$_4$]$_2$, indicating a large equilibrium constant for the formation of **10**. Crystals of **10** were obtained from slow diffusion of pentane into a toluene solution, and the molecular structure was determined by X-ray diffraction. An important structural feature of **10** is the presence of a semibridging carbonyl ligand supported by a Co-Rh single bond. The semibridging carbonyl results from the filled rhodium dπ donating into the π* of CO (Figure 7). The dπ to π* donation is reflected in the structure by an increased carbon-oxygen bond length for the semibridging CO (1.169 Å) compared to the average bond length of the terminal carbonyls (1.140 Å). DFT calculations (B3LYP, 3-21G/6-31G*)[39] for **10** converge to an energy-minimized structure that mimics the observed bridging CO unit (Figure 8). Analysis of the Mulliken atomic charges from the DFT shows a smaller positive charge on the semibridging carbonyl (C = 0.206, O = −0.305) compared to that of the terminal carbonyls (C_{avg} = 0.308, O_{avg} = −0.281), which is consistent with the bonding model. The infrared spectrum of **10** in a KBr pellet has a peak at 1820 cm^{-1} that is attributed to the CO stretching vibration of the semibridging carbonyl. The analogous porphyrin complex (OEP)Rh-Co-(CO)$_4$ shows only terminal CO stretches (ν_{CO} = 2054, 1996, and 1965 cm^{-1}) in the infrared spectrum.

Solutions of **10** in pyridine with a small excess of $[Co(CO)_4]_2$ immediately disproportionate into $[(tmtaa)Rh\text{-}(pyr)_2]^+$ and the cobalt tetracarbonyl anion (eq 14). Disproportionation is not observed by ^1H NMR for $[(tmtaa)\text{-}Rh]_2$ in pyridine, but **1** reacts via heterolytic pathways when treated with pyridinium chloride to form $[(tmtaa)Rh\text{-}(pyr)_2]^+[Cl]^-$ and (tmtaa)Rh-H. The cationic fragment $[(tmtaa)Rh(pyr)_2]^+$ shows an identical set of peaks with either cobalt tetracarbonyl or chloride anion, and the cobalt tetracarbonyl anion is observed by the FTIR (KBr pellet) T_2 CO stretching mode centered at 1880 cm^{-1} diagnostic of $Co(CO)_4^-$.[43,44]

$$(tmtaa)\,Rh\text{-}\,Co\,(\mu\text{-}\,CO)\,(CO)_3 + 2pyr \rightleftharpoons [(tmtaa)\,Rh(pyr)_2]^+ + [Co(CO)_4]^- \quad (14)$$

Solutions of **10** were charged with 200 Torr of ethene, resulting in the formation of an insoluble product that formed crystals in an NMR tube that were then used to obtain the molecular structure by X-ray diffraction (Figure 9). The product of the reaction of **10** with ethene is an ionic species with a cationic (tmtaa)Rh fragment, in which a CH_2CH_2 group bridges the rhodium and methine carbon centers, and a $[Co(CO)_4]^-$ counteranion. The diiminato fragment bridged to rhodium lost the delocalized π system, which is demonstrated in the structure by shorter N-C double bonds and longer C–C single bonds as shown in Figure 9. The nucleophilicity of the methine position was previously reported by Cotton.[45]

Formation and Reactions of (tmtaa)Rh-Mn(CO)$_5$

Reaction of $[(tmtaa)Rh]_2$ (**1**) with an excess of $[Mn(CO)_5]_2$ (**6**) in toluene proceeds in the dark over several weeks to achieve equilibrium with (tmtaa)Rh-$Mn(CO)_5$ (**11**) (eq 15), or **11** may be formed much more rapidly by photolysis (Rayonet RMR-400 photochemical reactor, 300 nm source).

$$[(tmtaa)\,Rh]_2 + [Mn(CO)_5]_2 \rightleftharpoons 2\,(tmtaa)\,Rh\text{-}\,Mn(CO)_5 \quad (15)$$

The molecular structure of **11** determined by X-ray diffraction shows only terminal CO ligands (Figure 10). The carbon monoxide trans to rhodium has shorter Mn-C (0.06 Å) and longer C–O (0.01 Å) bond lengths compared to that of the cis-oriented carbonyl, which is ascribed to larger π backbonding for the Mn-CO unit trans to rhodium. Infrared spectroscopy also shows only terminal CO stretches for **11** (1950–2150 cm^{-}1).

SUMMARY AND CONCLUSIONS

Transition metal complexes that are sources of d^5, d^7, and d^9 17-electron metal-centered radicals, including $[CpCr(CO)_3]_2$, $[CpMo(CO)_3]_2$, $[CpFe(CO)_2]_2$, $[Co(CO)_4]_2$, and $[Mn(CO)_5]_2$, react with rhodium(II) Dibenzotetramethylaza[14]-annulene dimers to form (tmtaa)Rh-M complexes (M = $CrCp(CO)_3$, $MoCp(CO)_3$, $FeCp(CO)_2$, $Co(CO)_4$, and $Mn(CO)_5$). The molecular structures for (tmtaa)Rh-$FeCp(CO)_2$, (tmtaa)Rh-$Co(\mu\text{-}CO)(CO)_3$, and (tmtaa)Rh-$Mn(CO)_5$ were determined by single crystal X-ray diffraction. The structure of (tmtaa)Rh-$Co(\mu\text{-}CO)(CO)_3$ has a semibridging carbon monoxide supported by a Rh-Co

bond. DFT calculations correctly mimic the observed bridging CO in (tmtaa)Rh-Co(μ-CO)-$(CO)_3$ and anticipate this type of bridging CO unit in (tmtaa)Rh-$CrCp(CO)_3$ and (tmtaa)Rh-$MoCp(CO)_3$, for which molecular structures could not be obtained. Equilibrium constants evaluated for the metathesis reactions show that the processes are nearly free energy neutral with $\Delta G°$ (298 K) varying in the range from +0.9 to +1.5 kcal mol^{-1}. Measurements of reaction equilibria permit the estimation of several (tmtaa)Rh-M bond dissociation enthalpies (Rh—Cr = 19 kcal mol^{-1}, Rh—Mo = 25 kcal mol^{-1}, and Rh—Fe = 27 kcal mol^{-1}). Several of the (tmtaa)Rh-M derivatives (M = $CpCr(CO)_3$ (**7**), $CpMo(CO)_3$ (**8**), and $Mn(CO)_5$ (**11**)) react with synthesis gas (1:1 CO/H_2) at 1 atm and 298 K to form (tmtaa)Rh-CHO and M-H derivatives, which makes these systems potential candidates for hydrogenation of the rhodium formyl unit under more forceful conditions.

Supplementary Material

Refer to Web version on PubMed Central for supplementary material.

Acknowledgments

This research was supported by the National Science Foundation through Grant CHE-1362016 and assisted by major research instrumentation Grant CNS-09-58854.

References

1. Imler GH, Bhagan S, Coffin VL, Wayland BB. Inorg Chem. 2012; 51:3352. [PubMed: 22375629]
2. Imler GH, Zdilla MJ, Wayland BB. Inorg Chem. 2013; 52:11509. [PubMed: 24004457]
3. Imler GH, Zdilla MJ, Wayland BB. J Am Chem Soc. 2014; 136:5856. [PubMed: 24724571]
4. Anderson DJ, Eisenberg R. Inorg Chem. 1994; 33:5378.
5. Wayland BB, Sherry AE, Poszmik G, Bunn AG. J Am Chem Soc. 1992; 114:1673.
6. Wayland BB. Polyhedron. 1988; 7:1545.
7. Wayland BB, Sherry AE, Bunn AG. J Am Chem Soc. 1993; 115:7675.
8. Wayland BB, Vanvoorhees SL, Wilker C. Inorg Chem. 1986; 25:4039.
9. Farnos MD, Woods BA, Wayland BB. J Am Chem Soc. 1986; 108:3659.
10. Wei ML, Wayland BB. Organometallics. 1996; 15:4681.
11. Bunn AG, Wei ML, Wayland BB. Organometallics. 1994; 13:3390.
12. Van Voorhees SL, Wayland BB. Organometallics. 1987; 6:204.
13. Fu XF, Basickes L, Wayland BB. Chem Commun (Cambridge, UK). 2003:520.
14. Bunn AG, Ni YP, Wei ML, Wayland BB. Inorg Chem. 2000; 39:5576. [PubMed: 11154576]
15. Fu X, Li S, Wayland BB. Inorg Chem. 2006; 45:9884. [PubMed: 17112286]
16. Fu XF, Wayland BB. J Am Chem Soc. 2005; 127:16460. [PubMed: 16305232]
17. Zhang X-X, Parks GF, Wayland BB. J Am Chem Soc. 1997; 119:7938.
18. West NM, Miller AJM, Labinger JA, Bercaw JE. Coord Chem Rev. 2011; 255:881.
19. Elowe PR, West NM, Labinger JA, Bercaw JE. Organometallics. 2009; 28:6218.
20. Hidai M, Fukuoka A, Koyasu Y, Uchida Y. J Mol Catal. 1986; 35:29.
21. Li C, Widjaja E, Garland M. Organometallics. 2004; 23:4131.
22. Rida MA, Smith AK. J Mol Catal A: Chem. 2003; 202:87.
23. Green JC, Green MLH, Parkin G. Chem Commun (Cambridge, UK). 2012; 48:11481.
24. Labinger JA. Inorg Chim Acta. 2015; 424:14.
25. Baird MC. J Organomet Chem. 2014; 751:50.
26. Pugh JR, Meyer TJ. J Am Chem Soc. 1992; 114:3784.

27. Woska DC, Ni YP, Wayland BB. Inorg Chem. 1999; 38:4135.
28. Klingler RJ, Rathke JW. J Am Chem Soc. 1994; 116:4772.
29. Bitterwolf TE. Coord Chem Rev. 2000; 206:419.
30. Stolzenberg AM, Cao Y. J Am Chem Soc. 2001; 123:9078. [PubMed: 11552815]
31. Li S, de Bruin B, Peng CH, Fryd M, Wayland BB. J Am Chem Soc. 2008; 130:13373. [PubMed: 18781751]
32. Coffin VL, Brennen W, Wayland BB. J Am Chem Soc. 1988; 110:6063. [PubMed: 22148782]
33. Wayland BB, Coffin VL, Farnos MD. Inorg Chem. 1988; 27:2745.
34. Koenig T, Finke RG. J Am Chem Soc. 1988; 110:2657.
35. Koenig TW, Hay BP, Finke RG. Polyhedron. 1988; 7:1499.
36. Koenig, T.; Scott, TW.; Franz James, A. Bonding Energetics in Organometallic Compounds. Vol. 428. American Chemical Society; Washington, DC: 1990. p. 113
37. Ng FTT, Rempel GL, Mancuso C, Halpern J. Organometallics. 1990; 9:2762.
38. Halpern J. Polyhedron. 1988; 7:1483.
39. Frisch, MJ.; Trucks, GW.; Schlegel, HB.; Scuseria, GE.; Robb, MA.; Cheeseman, JR.; Scalmani, G.; Barone, V.; Mennucci, B.; Petersson, GA.; Nakatsuji, H.; Caricato, M.; Li, X.; Hratchian, HP.; Izmaylov, AF.; Bloino, J.; Zheng, G.; Sonnenberg, JL.; Hada, M.; Ehara, M.; Toyota, K.; Fukuda, R.; Hasegawa, J.; Ishida, M.; Nakajima, T.; Honda, Y.; Kitao, O.; Nakai, H.; Vreven, T.; Montgomery, JA., Jr; Peralta, JE.; Ogliaro, F.; Bearpark, M.; Heyd, JJ.; Brothers, E.; Kudin, KN.; Staroverov, VN.; Kobayashi, R.; Normand, J.; Raghavachari, K.; Rendell, A.; Burant, JC.; Iyengar, SS.; Tomasi, J.; Cossi, M.; Rega, N.; Millam, JM.; Klene, M.; Knox, JE.; Cross, JB.; Bakken, V.; Adamo, C.; Jaramillo, J.; Gomperts, R.; Stratmann, RE.; Yazyev, O.; Austin, AJ.; Cammi, R.; Pomelli, C.; Ochterski, JW.; Martin, RL.; Morokuma, K.; Zakrzewski, VG.; Voth, GA.; Salvador, P.; Dannenberg, JJ.; Dapprich, S.; Daniels, AD.; Farkas, Ö.; Foresman, JB.; Ortiz, JV.; Cioslowski, J.; Fox, DJ. Gaussian 09, revision B.1. Gaussian Inc; Wallingford, CT: 2009.
40. Kiss G, Zhang K, Mukerjee SL, Hoff CD, Roper GC. J Am Chem Soc. 1990; 112:5657.
41. Tilset M, Parker VD. J Am Chem Soc. 1989; 111:6711.
42. Tilset M, Parker VD. J Am Chem Soc. 1990; 112:2843.
43. Friedel RA, Wender I, Shufler SL, Sternberg HW. J Am Chem Soc. 1955; 77:3951.
44. Fumagalli A, Ulivieri P, Costa M, Crispu O, Della Pergola R, Fabrizi de Biani F, Laschi F, Zanello P, Macchi P, Sironi A. Inorg Chem. 2004; 43:2125. [PubMed: 15018536]
45. Cotton FA, Czuchajowska-Wiesinger J. Gazz Chim Ital. 1992; 122:321.

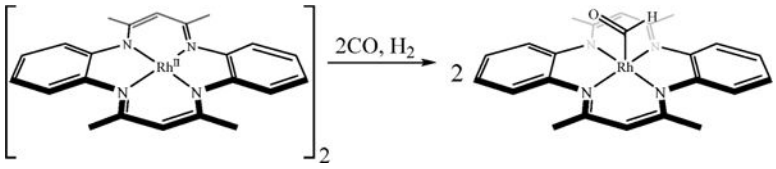

Figure 1.
Reaction of $[(tmtaa)Rh]_2$ with CO and H_2.

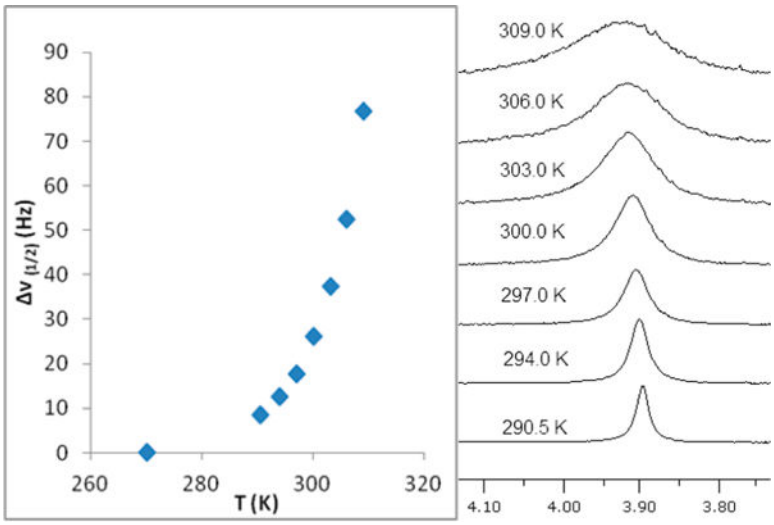

Figure 2.

Temperature dependence of the ^{1}H NMR line width for the cyclopentadienyl ligand in (tmtaa)Rh-CrCp(CO)$_3$.

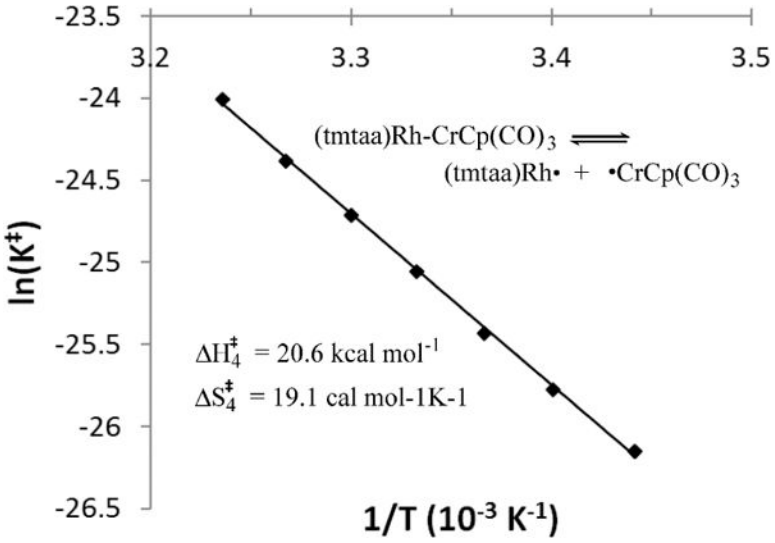

Figure 3.

Determination of activation parameters for homolytic dissociation of (tmtaa)Rh-CrCp(CO)$_3$ into (tmtaa)Rh● and (CO)$_3$CpCr● in d_8-toluene by ^{1}H NMR line width measurements of the cyclopentadienide hydrogens ($\Delta H^{\ddagger}_4$ = 21 (1) kcal mol^{-1}, $\Delta S^{\ddagger}_{ex,4}$ = 19.6 (1.2) cal K^{-1} mol^{-1}).

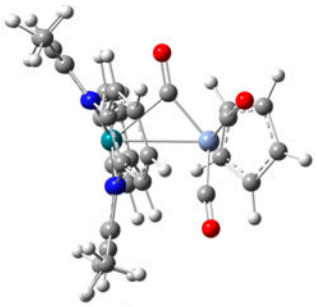

	internuclear distance (Å) DFT
Rh-Cr	2.96
C-O (bridging)	1.175
Cr-C (bridging)	1.915
Rh-C (bridging)	2.222
C-O (terminal)	1.162
Cr-C (terminal)	1.846
Rh-N (avg)	2.05

Figure 4.
Minimum energy structural optimization of (tmtaa)Rh-CrCp(CO) by DFT (B3LYP, 3-21G/6-31G*) and a table of selected internuclear distances.

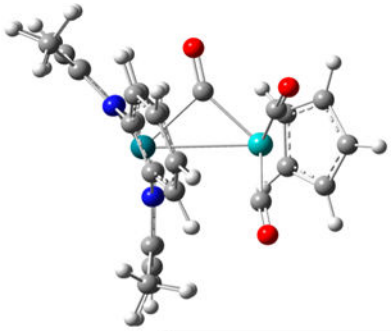

	internuclear distance (Å) DFT
Rh-Mo	3.032
C-O (bridging)	1.175
Mo-C (bridging)	2.057
Rh-C (bridging)	2.189
C-O (terminal)	1.162
Mo-C (terminal)	1.972
Rh-N (avg)	2.049

Figure 5.

Minimum energy structural optimization of (tmtaa)Rh-MoCp(CO)$_3$ by DFT (B3LYP, 3-21G/6-31G*) and a table of selected internuclear distances.

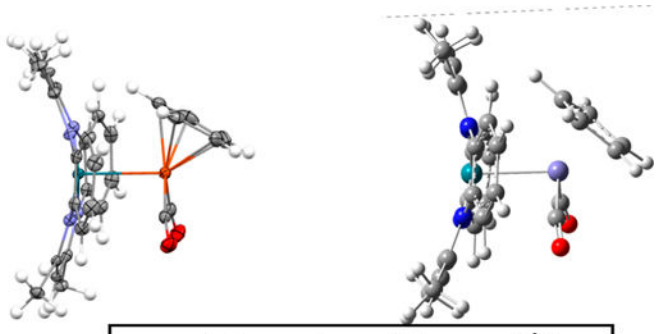

	internuclear distance (Å)	
	Crystal	DFT
Rh-Fe	2.632	2.607
C-O (avg)	1.150	1.156
Fe-C (avg)	1.764	1.757
Rh-N (avg)	1.998	2.044

Figure 6.

ORTEP representation of (tmtaa)Rh-FeCp(CO)$_2$ (**9**) structure from single crystal X-ray diffraction with thermal ellipsoids shown on non-hydrogen atoms at 50% probability level, hydrogen atoms shown as open circles, and energy minimization by DFT computations (B3LYP, 3-21G/6-31G*). A table of selected internuclear distances observed in the molecular structure and calculated by DFT is also included.

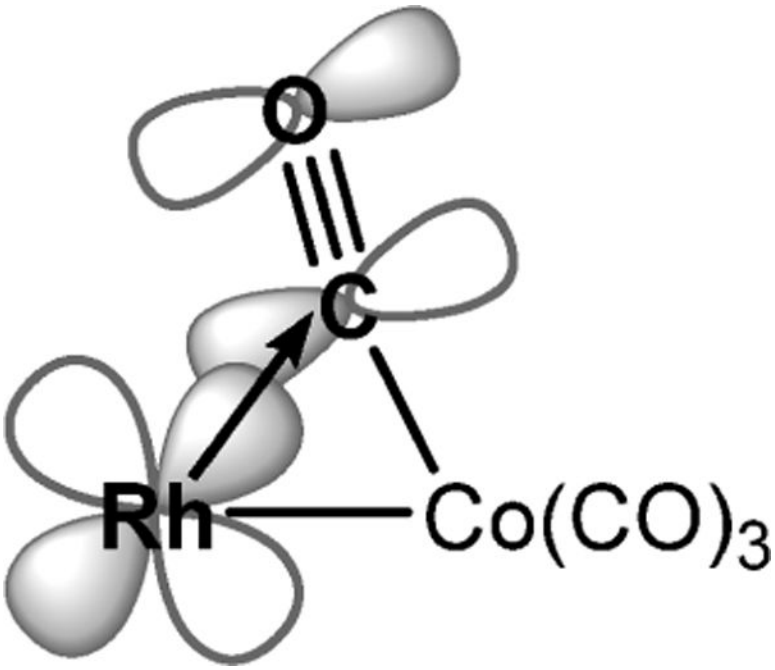

Figure 7.

Drawing of the semibridging carbonyl in (tmtaa)Rh-Co(μ-CO)$(CO)_3$ showing the donation of rhodium dπ into the C≡O π* orbital.

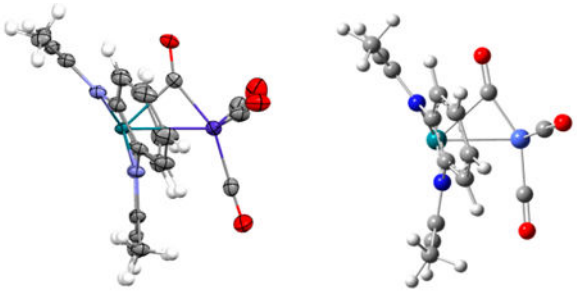

	internuclear distance (Å)	
	Crystal	DFT
Rh-Co	2.688	2.718
C-O (bridging)	1.169	1.172
Co-C (bridging)	1.838	1.819
Rh-C (bridging)	2.078	2.160
C-O (terminal)	1.140	1.152
Co-C (terminal)	1.796	1.778
Rh-N (avg)	1.996	2.042

Figure 8.

ORTEP representation of the (tmtaa)Rh-Co$(CO)_4$ structure from single crystal X-ray diffraction with thermal ellipsoids shown on non-hydrogen atoms at 50% probability level, hydrogen atoms shown as open circles, and energy minimization by DFT computations (B3LYP, 3-21G/6-31G*). A table of selected internuclear distances observed in the molecular structure and calculated by DFT is also included.

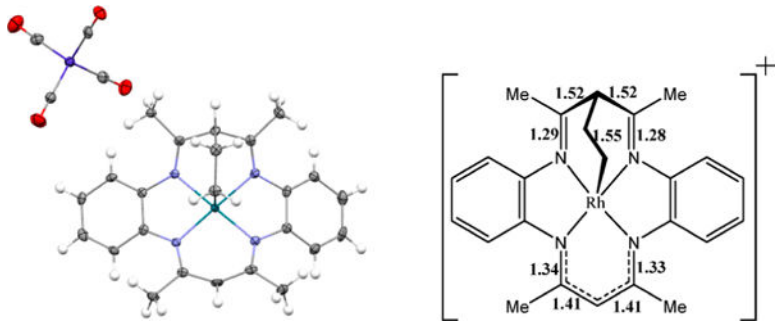

Figure 9.

Crystal structure of ionic bridged ethyl complex and drawing of cationic (tmtaa)Rh fragment with bond distances labeled in angstroms.

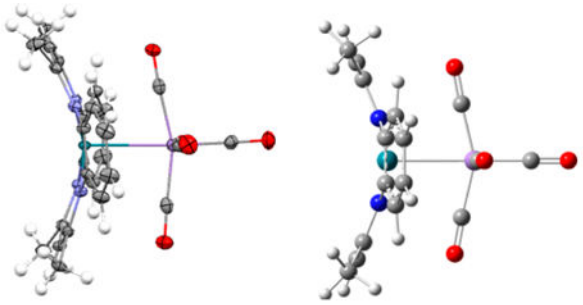

	internuclear distance (Å)	
	Crystal	DFT
Rh-Mn	2.711	2.726
C-O (cis, avg)	1.138	1.15
C-O (trans)	1.149	1.156
Mn-C (cis, avg)	1.864	1.853
Mn-C (trans)	1.800	1.793
Rh-N (avg)	2.000	2.05

Figure 10.

ORTEP representation of the (tmtaa)Rh-Mn$(CO)_5$ structure from single crystal X-ray diffraction with thermal ellipsoids shown on non-hydrogen atoms at 50% probability level, hydrogen atoms shown as open circles, and energy minimization by DFT computations (B3LYP, 3-21G/6-31G*). A table of selected internuclear distances observed in the molecular structure and calculated by DFT is also included.